INORGANIC CHEMISTRY FRONTIERS

RESEARCH ARTICLE

View Article Online
View Journal | View Issue

Cite this: *Inorg. Chem. Front.*, 2023, **10**, 3319

Quasi-linear CuX_2 (X = Cl, Br) motif-built hybrid copper halides realizing encouraging nonlinear optical activities†

Jing-Li Qi, Jiajing Wu,* Yue Guo, Zhong-Ping Xu, Wenlong Liu and Sheng-Ping Guo *

Received 17th February 2023,
Accepted 24th April 2023

DOI: 10.1039/d3qi00297g

rsc.li/frontiers-inorganic

The emerging organic–inorganic hybrid metal halides feature unique optical and electronic properties, are easily grown and have flexible crystal structures, making them a class of promising next-generation nonlinear optical (NLO) and ferroelectric materials. Herein, we successfully synthesized two centimeter-level zero-dimensional copper halide organic–inorganic hybrids $(C_{20}H_{20}P)CuX_2$ (X = Cl, Br) that are crystallized in the monoclinic noncentrosymmetric $P2_1$ space group. Their structures contain rare quasi-linear $[CuX_2]^-$ anions and $[C_{20}H_{20}P]^+$ cations. $(C_{20}H_{20}P)CuCl_2$ and $(C_{20}H_{20}P)CuBr_2$ crystals show phase-matchable NLO effects around 1.1 and 0.87 times that of benchmark KDP, respectively. These $(C_{20}H_{20}P)CuX_2$ materials are the first NLO-active examples in the hybrid copper(I) halide family containing a quasi-linear CuX_2 unit.

Introduction

As a type of significant nonlinear optical (NLO) response, second-harmonic generation (SHG) is widely used for laser frequency conversion, which is the foundation for a range of advanced applications, such as laser manufacturing, laser guidance, live-cell imaging, telecommunication and military technologies.[1–6] To date, many SHG materials are applied from the deep ultraviolet to infrared regions, including KH_2PO_4 (KDP),[7] $KTiOPO_4$ (KTP),[8] β-BaB_2O_4 (β-BBO),[9] $KBe_2BO_3F_2$ (KBBF),[10] $AgGaS_2$ (AGS),[11] $AgGaSe_2$ [12] and $ZnGeP_2$.[13] Although they can satisfy the requirements of the market to a certain extent, they are still plagued with several inherent defects. For example, AGS exhibits low laser-induced damage thresholds (LIDTs), $AgGaSe_2$ shows non-phase-matching, and $ZnGeP_2$ suffers from strong two-photon absorption, which severely limit their practical application. Therefore, exploring new high-performance NLO materials is imperative in science and technology.

Organic–inorganic hybrid metal halides, as a new type of photoelectric functional material with diverse structures and low-temperature solution processability, have attracted much attention owing to their great advances in photovoltaic devices, solid-state lasers, lighting and displays in recent years.[14–16] In particular, with different combinations of organic components and metal cations (Cu^+, Pb^{2+}, Sn^{2+}, Zn^{2+}, Cd^{2+}, Hg^{2+}, Cu^{2+}, Bi^{3+}, Sb^{3+}, In^{3+}, *etc.*), a great number of hybrid metal halides have been explored as promising materials for various NLO applications owing to their fascinating advantages of inorganic metal frameworks and organic molecules.[17–22] Inspired by the classic three-dimensional (3D) metal halide perovskite prototype AMX_3 (A = organic cations, M = bivalent metal cation, and X = halogen anion), bivalent metal cations are replaced by heterovalent metal ions to form perovskite-like derivatives and MX_n (n = 2, 3, 4, 5) units with different coordination numbers. Among the perovskite-like derivatives, a linear structure $[MX_2]$ unit is very rarely discovered, though they have demonstrated inherent advantages to achieve large SHG effects and birefringence attributed to their relatively large polarities and the ordered arrangement of linear anionic groups. Regrettably, of the previously reported NLO metal halides, only Hg-based halides, such as $HgBr_2$ and β-HgBrCl, have shown evidence of these advantages. However, the intrinsic toxicity of the Hg^{2+} ion hampers their further commercial application.[23,24] To address this drawback, Wu *et al.* first obtained two hybrid halides $[N(CH_3)_4MCl_2$ (M = In, Ga)] containing MCl_2 linear units in 2020, which presented good SHG behaviors.[25] Therefore, it is attractive to develop new linear $[MX_2]$ units as promising building blocks for hybrid nonlinear optical materials.

Environmentally friendly copper is a promising optoelectronic element due to its abundance, low price, and flexibility in structure, composition, and stoichiometry. The Cu(I) ion with a small ionic size of 0.6 Å may be surrounded by two,

School of Chemistry and Chemical Engineering, Yangzhou University, Yangzhou, Jiangsu 225002, P. R. China. E-mail: spguo@yzu.edu.cn, jiajingw@yzu.edu.cn

†Electronic supplementary information (ESI) available: Additional tables and pictures. CCDC 2195572 and 2195573. For ESI and crystallographic data in CIF or other electronic format see DOI: https://doi.org/10.1039/d3qi00297g

three or four halide ions to form $[CuX_2]$, $[CuX_3]$ or $[CuX_4]$ configurations. In recent years, although hybrid copper halides containing $[CuX_2]$ linear structures have been reported, most of them adopt centrosymmetric (CS) structures due to the antiparallel arrangement of the $[CuX_2]$ units.[26–31] Furthermore, the exploration of NLO properties in hybrid copper halides with linear units in reported noncentrosymmetric (NCS) structures is lacking.[32–34] Therefore, it remains a challenge to design and synthesize Cu(I)-based hybrids with linear units $[CuX_2]$ and phase-matchable NLO behaviour. In this study, by assembling an asymmetric organic molecule $[(C_6H_5)_3PC_2H_5X]$ with a d^{10} transition-metal cation, we obtained two polar low-toxicity copper(I) halide materials, $(C_{20}H_{20}P)CuX_2$ (X = Cl (**1**), Br (**2**)), which are composed of a quasi-linear $[CuX_2]^-$ unit and $[C_{20}H_{20}P]^+$ cations. Although the crystal structure of **2** was reported in 1985, its NLO property has never been studied.[32] Both **1** and **2** crystallize in the polar space group $P2_1$ with good SHG responses. Specifically, this is the first work addressing NLO activity in the Cu(I)-based hybrids family containing quasi-linear $[CuX_2]^-$ units. Their electronic structures and optical properties were also calculated based on DFT theory. We believe that this work will pave the way for designing organic–inorganic hybrid NLO materials with good SHG efficiency and sufficient birefringence for all-solid-state lasers.

Experimental section

Materials

Copper(I) chloride (CuCl, 97%, Aladdin), copper(I) bromide (CuBr, 99%, Aladdin), ethyltriphenylphosphonium bromide ($C_{20}H_{20}PBr$, 98%, Adamas), ethyltriphenylphosphonium chloride ($C_{20}H_{20}PCl$, 98%, Aladdin), HCl (36 wt% in H_2O, AR), ethylene glycol (≥99.5%, Sinopharm), HBr (40 wt% in H_2O, AR), H_3PO_2 (36 wt% in H_2O, Aladdin) were purchased and used without further purification.

Syntheses

$(C_{20}H_{20}P)CuX_2$ (X = Cl, Br): $C_{20}H_{20}PX$ (1 mmol), CuX (0.5 mmol) were dissolved in ethylene glycol (6–8 ml), HX (1 ml) and H_3PO_2 (0.3 ml) at 80 °C with stirring to form a clear solution. By naturally cooling the above mixture for 12 h, large-sized rod-like crystals were obtained.

Characterizations

The crystallography data of $(C_{20}H_{20}P)CuX_2$ (X = Cl, Br) were collected using a Bruker D8 QUEST X-ray diffractometer with graphite-monochromated Mo-Kα radiation (λ = 0.71073 Å). The crystal structures were solved by direct methods and refined by full-matrix least-squares techniques on F^2 with anisotropic displacement parameters for all atoms.[35] The CIF documents of $(C_{20}H_{20}P)CuX_2$ (X = Cl, Br) are also deposited with the CCDC numbers of 2195572–2195573.† The purity of the compounds were confirmed by powder X-ray diffraction (Bruker D8 Advance) at 40 kV and 100 mA with Cu-Kα radiation (λ = 1.5406 Å) with a scan speed of 5° min^{-1} at room temperature within the range of 2θ = 5–80°. An energy dispersive X-ray spectroscope (EDS, Zeiss-Supra55) was used for microprobe elemental analyses.

UV-vis absorption spectra were collected using a Varian Cary 5000 at room temperature within the range 200–800 nm. The SHG measurement on powdery crystalline samples of $(C_{20}H_{20}P)CuX_2$ (X = Cl, Br) was tested using a modified Kurtz–Perry NLO system[36] with 1.064 μm Q-switch laser radiation as the light source. The powder samples were sieved into six different ranges, including 26–45, 45–90, 90–150, 150–200, 200–250 and 250–315 μm to measure their size-dependent SHG responses. The SHG signals were collected by a photomultiplier tube and the peaks were shown on the oscilloscope.

Theoretical calculations

Single-crystal structural data of $(C_{20}H_{20}P)CuX_2$ (X = Cl, Br) were used for the theoretical calculations. The electronic structures and optical properties were calculated using a plane-wave basis set and *pseudo*-potentials within the total-energy code CASTEP based on density functional theory (DFT).[37] The Perdew–Burke–Ernzerhof (PBE) functional under the generalized gradient approximation (GGA) was chosen to treat the exchange–correlation potential.[38] The interactions between the ionic cores and the electrons were described by the norm-conserving pseudopotential. The following valence-electron configurations were considered in the computation: Cu: $4s^13d^{10}$, Cl: $3s^23p^5$, Br: $4s^24p^5$, C: $2s^22p^2$, P: $2s^22p^3$, and H: $1s^1$. A plane-wave cutoff energy of 440 eV and a 3 × 2 × 3 grid of Monkhorst–Pack points were employed for band structures and density of states, which ensure good convergence of the computed structures and energies. The other parameters and convergence criteria are default values for the CASTEP code. The optical properties were calculated in terms of the real ($\varepsilon_1(\omega)$) and imaginary ($\varepsilon_2(\omega)$) parts of complex dielectric function $\varepsilon(\omega)$, $\varepsilon(\omega) = \varepsilon_1(\omega) + i\varepsilon_2(\omega)$.[39] The first-order nonresonant susceptibility of the low-frequency region is $X^1(\omega) = \varepsilon_1(\omega) - 1$, and the SHG tensors can be expressed in terms of the first-order susceptibilities as follows:[40]

$$X^{(2)}_{ijk}(\omega_1, \omega_2, \omega_3) = \frac{ma}{N^2e^3} X^{(1)}_{ii}(\omega_3) X^{(1)}_{jj}(\omega_1) X^{(1)}_{kk}(\omega_2) \quad (1)$$

Where m, e and N are the electron mass, electron charge and number density of the atom respectively, and parameter a is the nonlinear response. The refractive index n was calculated based on the following formula:

$$n(\omega) = \frac{1}{\sqrt{2}} \left\{ \left[\varepsilon_1(\omega)^2 + \varepsilon_2(\omega)^2\right]^{1/2} + \varepsilon_1(\omega) \right\}^{1/2}. \quad (2)$$

Results and discussion

Crystal structures

Single crystals of **1** and **2** were prepared by slow cooling clear solutions containing CuX and $C_{20}H_{20}PX$ with a 0.5 : 1 molar ratio from 80 °C to room temperature. Fig. 1a shows the syn-

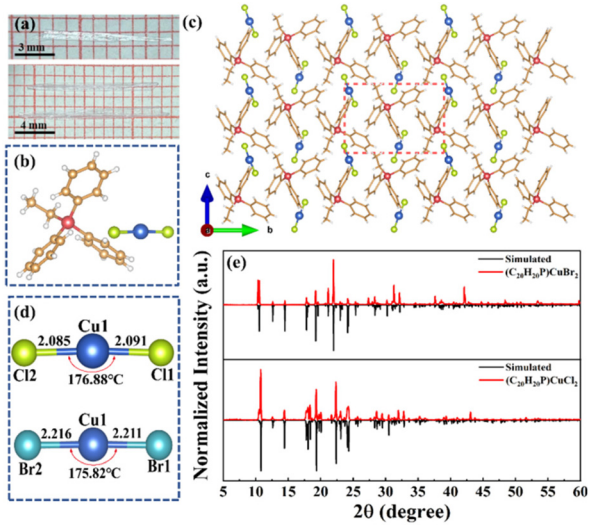

Fig. 1 (a) Photographs of **1** (top) and **2** (bottom) crystals in sunlight. (b) Asymmetric unit of **1**. (c) Crystal structure of **1**. (d) Coordination environment of a Cu^{+} cation. (e) Experimental and simulated powder X-ray diffraction patterns of **1** and **2**.

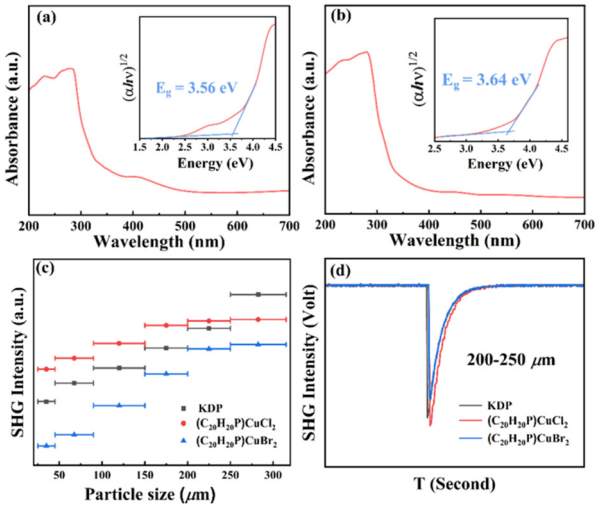

Fig. 2 Absorption spectra of (a) $(C_{20}H_{20}P)CuCl_2$ and (b) $(C_{20}H_{20}P)CuBr_2$. The insets are the optical band gaps obtained from Tauc plots. (c) SHG intensity with different particle sizes and (d) the oscilloscope trace of the SHG signal of $(C_{20}H_{20}P)CuX_2$ (X = Cl, Br) and KDP in the same particle-size range of 200–250 μm.

thesized single crystals with sizes up to 12 mm. Structure analyses reveal that **1** and **2** crystallize in the monoclinic system with an NCS space group $P2_1$ (polar point group 2). The formation of the NCS structures is attributed to the volume difference of the phenyl and ethyl groups of the organic cation, which makes the linear units form a non-antiparallel arrangement in the unit cell (Fig. S2†). Detailed crystal and structure refinement parameters are shown in Tables S1–S4.† Energy-dispersive X-ray spectroscopy (EDS) analysis indicates that the atomic ratios of X : Cu : P in both **1** and **2** are around 2 : 1 : 1 (Fig. S4†), which are consistent with the results of crystal-structure analysis. As **1** and **2** are isostructural, the structure of **1** will be discussed as a representative. Within the asymmetric unit, **1** is composed of one organic $[C_{20}H_{20}P]^{+}$ cation and one inorganic $[CuCl_2]^{-}$ anion (Fig. 1b). Each central Cu atom is coordinated with two Cl atoms to form a quasi-linear $[CuCl_2]^{-}$ unit, and the $[CuCl_2]^{-}$ units are embedded periodically in the matrix of organic $[C_{20}H_{20}P]^{+}$ cations (Fig. 1c). It's worth noting that the configuration of Cl–Cu–Cl (176.88°) is quasi-linear, slightly deviating from the ideal linear. Compared to **2**, the Cu–X bond lengths in **1** are decreased from 2.211(9) to 2.091 (1) Å (Fig. 1d). The nearest distance of Cu···Cu in **1** is 6.482 Å (Fig. S3†). It's noteworthy that most of the previously reported copper halides containing linear copper–halide units crystallized in the CS space groups, and linear anionic halide frameworks have been rarely reported until now.[32–34,41,42] The phase purities of **1** and **2** were verified by powder X-ray diffraction (XRD) analysis, which are in good agreement with the simulated ones (Fig. 1e).

Optical measurements

To study the optical properties of **1** and **2**, absorption spectra were measured and are shown in Fig. 2a and b. The corresponding band gaps determined from Tauc plots are 3.56 eV for **1**, and 3.64 eV for **2**, which are consistent with their crystals' color and close to the range of 3.4–4 eV found for most previously reported copper halides (Table S8†). However, it is worth noting that two works report that the band gaps of similar structures are smaller than this range, which is due to the long absorption tail of the absorption spectra.[26,29] By comparing the absorption spectra, it can be found that the above two works use the absorption edge of the weak peak on the absorption tail to determine the band gap. In this work, the band gaps of 3.56 and 3.64 eV are reasonable when considering the colorless and transparent nature of the crystals. Like previously reported copper halides containing $[CuX_2]$ units (Table S8†), **1** and **2** exhibit photoluminescence under UV light. The photoluminescence excitation (PLE) and photoluminescence (PL) spectra of **1** and **2** are shown in Fig. S7a and S7b,† and the emission peaks of **1** and **2** are located at 523 and 533 nm, respectively. Owing to their structural asymmetry, the powder SHG responses of **1** and **2** were investigated by the Kurtz and Perry method under 1064 nm laser radiation with KDP as the reference. As shown in Fig. 2c, their SHG intensities increase with the particle sizes, indicating that they are phase-matchable. And in the particle size range of 200–250 μm, their SHG intensities are about 1.1 (**1**) and 0.89 (**2**) times that of KDP. The results are much stronger than those of most organic–inorganic hybrid lead-free metal halides, such as $[N(C_2H_5)_4]InCl_{4-x}Br_x$ (0.5–0.8 × KDP),[43] $[TEA]_2MnBr_4$ (0.48 × KDP),[44] $[BTMA]_2MnBr_4$ (0.59 × KDP),[44] $(C_6H_{14}N)_2SbCl_5$ (0.3 × KDP),[45] $[NH_3CH_2CH_2F]_3BiCl_6$ (0.6 × KDP),[46] and $(C_4H_{16}N_3)BiBr_6$ (0.6 × KDP).[47]

To further evaluate the SHG contribution for **1** and **2**, the net dipole moments (DM) within a unit cell were calculated *via* a previously reported method (Fig. S6 and Table S6†).[44]

We suppose that the dipole centers of the positive charges of the $[C_{20}H_{20}P]^+$ cations and the negative charges of the $[CuX_2]^-$ anions are located at the P and Cu atoms, respectively. Thus, the average coordinates of P atoms are (0.5, 0.6808, 0.5) with the average coordinates of Cu atoms lying at (0.5, 0.2960, 0.5) in **1**. Obviously, the coordinates of electric charges are not a coincidence, thus, it will produce DM for **1**. According to $m = r \times q$, a DM (μ_{total}) of 48.68 D is obtained for **1**. Similarly, the calculated DM of **2** is 46.64 D. This is because the SHG response is inversely correlated to the volume (Ω) and the square of the band gap (E_g^2). A corrected total DM (μ_c) was quantified using the following equation: $\mu_c = \mu_{total}/(\Omega \times E_g^2)$.[48–50] As a result, μ_c of **1** is 0.0089 D/(Å^3 × eV^2), which is larger than 0.00513 D/(Å^3 × eV^2) of **2**, consistent with the experimental results.

Theoretical studies

To get more insights into the structure–property relationship of **1** and **2**, first-principles calculations were performed using the PBE functional (details given in Experimental section). As shown in Fig. 3a and c, the valence band (VB) and conduction band (CB) of the electronic structures for **1** and **2** are very dense and nearly flat, indicating that the electronic states are highly localized, and the electronic coupling is negligible. Thus, there is a strong quantum confinement effect and nearly no electronic interaction between adjacent inorganic anion units, which is consistent with the aforementioned results of large distance between the adjacent inorganic units. The DFT calculations for **1** and **2** give indirect band gaps of 2.43 and 3.15 eV, respectively, which are underestimated compared to the experimental optical band gaps of 3.56 eV for **1** and 3.64 eV for **2** (Fig. 2a and b) due to the errors in the PBE calculation.[26,51] The indirect band gaps of **1** and **2** make them only weakly photoluminescent, which is different from the previously reported bright photoluminescence of copper halides with direct bandgaps.[29–31] The density of states (DOS) of **1** shows that the valence band maximum (VBM) consists of Cu 3d and Cl 3p orbitals, and the conduction band minimum (CBM) located consists of orbitals from the organic unit $[C_{20}H_{20}P]^+$ (Fig. 3b). For **2**, the VBM is also derived from Cu 3d and Br 4p orbitals, while the CBM is still derived from the orbitals of the organic $[C_{20}H_{20}P]^+$ cation. However, the lowest conduction band changes from 1.71 to 2.55 eV, resulting in a larger band gap of **2**. As is known, the optical properties are mainly determined by the electron transition near the energy band gap, so it can be concluded that both the organic cations and inorganic anions contribute to the PL emission. This type of DOS has been widely reported in copper halides, suggesting that substituting organic cations and halogens can tune the electronic structure of copper halides, thereby tuning their optical properties.[28–32]

The space group $P2_1$ of **1** and **2** belongs to the point group 2 and has four non-vanishing independent SHG coefficients (d_{14}, d_{16}, d_{22} and d_{23}) under the restriction of Kleinman symmetry. The frequency-dependent SHG coefficients are plotted in Fig. 4a and c. The largest SHG coefficients at 1064 nm (1.165 eV) is 0.67 and 0.77 pm V^{-1} for **1** and **2**, respectively, in good agreement with the experimental values. In addition, Fig. 4b and d show the calculated refractive index dispersion curves, which exhibit strong anisotropic characteristics: $n_x \approx n_z > n_y$. The calculated n_x, n_y, and n_z are 1.750, 1.749, and 1.664, respectively. The birefringence (Δn) is 0.12 and 0.13 for **1** and **2**, respectively, at 1064 nm, large enough to achieve phase matching for the SHG process, which is consistent with the experimental phase-matchable behaviors. Indeed, **1** and **2** exhibit much larger birefringences than most of the reported SHG-active hybrid metal halides, such as $[N(CH_3)_4]InBr_2$ (0.038),[25] $[N(C_2H_5)_4]InX_4$ (X = Br, Cl) (0.01),[43] $(BTA)_3Bi_2Cl_9$ (0.086),[50] and $(C_9H_{14}N)SbCl_4$ (0.095).[52]

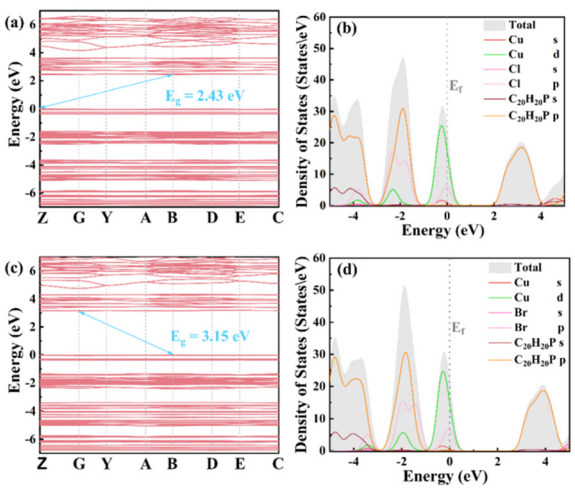

Fig. 3 The calculated band structures of (a) **1** and (c) **2**. Projected density of states of (b) **1** and (d) **2**.

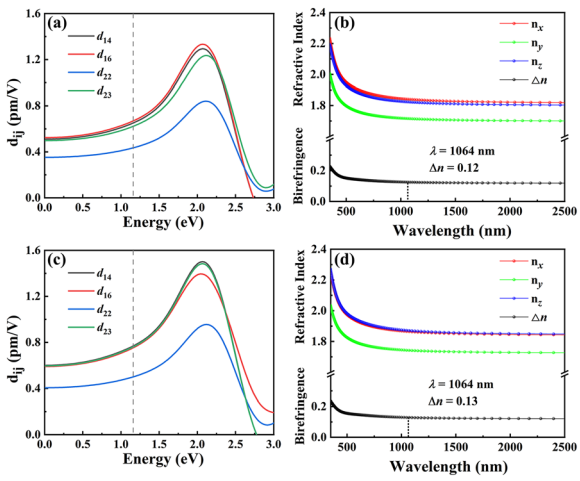

Fig. 4 Calculated frequency-dependent SHG coefficients of (a) **1** and (c) **2**; calculated frequency-dependent refractive index and birefringences of (b) **1** and (d) **2**.

Conclusions

In summary, a new type of NCS lead-free hybrid copper halide NLO crystal, $(C_{20}H_{20}P)CuX_2$ (X = Cl, Br), has been synthesized through a simple solution strategy in the atmospheric environment. The crystals exhibit phase-matchable SHG effects and suitable birefringences. Theory calculations reveal that the origin of the SHG response is triggered by a synergistic effect, which is the ordering of flexible organic cations $[C_{20}H_{20}P]^+$ and the inorganic $[CuX_2]^-$ anions. Our work provides new examples to enrich the structures of hybrid metal–halide systems and to investigate new types of NLO materials.

Author contributions

The manuscript was written through contributions of all authors. All authors have given approval to the final version of the manuscript.

Conflicts of interest

The authors declare that they have no conflict of interest.

Acknowledgements

This work was supported by the National Natural Science Foundation of China (22071212), Qinglan Project of Jiangsu Province of China, the Priority Academic Program Development of Jiangsu Higher Education Institutions, the Natural Science Foundation of Jiangsu Province (Grant No. BK20220558), Yangzhou University with a start-up grant (Grant No. 137012279) and the Lvyangjinfeng Talent Program of Yangzhou (YZLYJFJH2021YXBS085).

References

1 J. Chen, C. L. Hu, F. Kong and J. G. Mao, High-performance second-harmonic-generation (SHG) materials: new developments and new Strategies, *Acc. Chem. Res.*, 2021, **54**, 2775–2783.

2 K. M. Ok, Toward the rational design of novel noncentrosymmetric materials: factors Influencing the framework structures, *Acc. Chem. Res.*, 2016, **49**, 2774–2785.

3 X. Huang, S.-H. Yang, X.-H. Li, W. Liu and S.-P. Guo, $Eu_2P_2S_6$: the first rare-earth chalcogenophosphate exhibiting large Second-harmonic generation response and high laser-induced damage Threshold, *Angew. Chem., Int. Ed.*, 2022, **61**, e202206791.

4 N. Yoshikawa, T. Tamaya and K. Tanaka, High-harmonic generation in graphene enhanced by elliptically polarized light excitation, *Science*, 2017, **356**, 736–738.

5 N. L. B. Sayson, T. Bi, V. Ng, H. Pham, L. S. Trainor, H. G. L. Schwefel, S. Coen, M. Erkintalo and S. G. Murdoch, Octave-spanning tunable parametric oscillation in crystalline Kerr microresonators, *Nat. Photonics*, 2019, **13**, 701–706.

6 M. Yan, W. D. Yao, W. L. Liu, R. L. Tang and S. P. Guo, Helical $\{[HgS]\}_n$ chain-Induced balanced nonlinear-optical performance for trigonal mercury sulfide, *Inorg. Chem.*, 2021, **60**, 16917–16921.

7 Y. S. Liu, W. B. Jones and J. P. Chernoch, High–efficiency high–power coherent uv generation at 266 nm in 90° phase–matched deuterated KDP, *Appl. Phys. Lett.*, 1976, **29**, 32–34.

8 J. D. Bierlein and H. Vanherzeele, Potassium titanyl phosphate: properties and new applications, *J. Opt. Soc. Am. B*, 1989, **6**, 622–633.

9 C. T. Chen, B. Wu, A. Jiang and G. You, a new-type ultraviolet shg crystal—β-BaB_2O_4, *Sci. Sin., Ser. B*, 1985, **28**, 235–243.

10 B. Wu, D. Y. Tang, N. Ye and C. T. Chen, Linear and nonlinear optical properties of the $KBe_2BO_3F_2$ (KBBF) crystal, *Opt. Mater.*, 1996, **5**, 105–109.

11 A. K. Harasaki and K. Kato, New data on the nonlinear optical constant, phase-matching, and optical damage of $AgGaS_2$, *Jpn. J. Appl. Phys.*, 1997, **36**, 700–703.

12 G. C. Catella, L. R. Shiozawa, J. R. Hietanen, R. C. Eckardt, R. K. Route, R. S. Feigelson, D. G. Cooper and C. L. Marquardt, Mid-IR absorption in $AgGaSe_2$ optical parametric oscillator crystals, *Appl. Opt.*, 1993, **32**, 3948–3951.

13 G. D. Boyd, T. J. Bridges, C. K. N. Patel and E. Buehler, Phase-matched submillimeter wave generation by difference–frequency mixing in $ZnGeP_2$, *Appl. Phys. Lett.*, 1972, **21**, 553–555.

14 J. J. Xue, R. Wang, X. H. Chen, C. L. Yao, X. Y. Jin, K. L. Wang, W. C. Huang, T. Y. Huang, Y. P. Zhao, Y. X. Zhai, D. Meng, S. Tan, R. Z. Liu, Z. K. Wang, C. H. Zhu, K. Zhu, M. C. Beard, Y. F. Yan and Y. Yang, Reconfiguring the band-edge states of photovoltaic perovskites by conjugated organic cations, *Science*, 2021, **371**, 636–640.

15 J. Y. Tong, J. W. Luo, L. Shi, J. J. Wu, L. Y. Xu, J. M. Song, P. Wang, H. B. Li and Z. T. Deng, Fabrication of highly emissive and highly stable perovskite nanocrystal-polymer slabs for luminescent solar concentrators, *J. Mater. Chem. A*, 2019, **7**, 4872–4880.

16 H. Li, C. J. Pi, W. Q. Chen, M. Zhou, J. M. Wei, J. H. Yi, P. Song, Y. Alexey, Y. Zhong, X. Yu, J. B. Qiu and X. H. Xu, A highly stable photodetector based on a lead-free double perovskite operating at different temperatures, *J. Phys. Chem. Lett.*, 2021, **12**, 5682–5688.

17 D. Y. Fu, J. L. Xin, Y. Y. He, S. C. Wu, X. Y. Zhang, X. M. Zhang and J. H. Luo, Chirality-dependent second-order nonlinear optical effect in 1D organic–inorganic hybrid perovskite bulk single crystal, *Angew. Chem., Int. Ed.*, 2021, **60**, 20021–20026.

18 D. Chen, S. Q. Hao, L. B. Fan, Y. W. Guo, J. Y. Yao, C. Wolverton, M. G. Kanatzidis, J. Zhao and Q. L. Liu,

Broad photoluminescence and second-harmonic generation in the noncentrosymmetric organic–inorganic hybrid halide $(C_6H_5(CH_2)_4NH_3)_4MX_7{\cdot}H_2O$ (M = Bi, In, X = Br or I), *Chem. Mater.*, 2021, **33**, 8106–8111.

19 L. Yao, Z. X. S. Zeng, C. K. Cai, P. Xu, H. G. Gu, L. Gao, J. B. Han, X. W. Zhang, X. Wang, X. Wang, A. L. Pan, J. Wang, W. X. Liang, S. Y. Liu, C. Chen and J. Tang, Strong second- and third-harmonic generation in 1D chiral hybrid bismuth halides, *J. Am. Chem. Soc.*, 2021, **143**, 16095–16104.

20 Z. H. Guo, J. Z. Li, J. C. Liang, C. S. Wang, X. Zhu and T. C. He, Regulating optical activity and anisotropic second-harmonic generation in zero-dimensional hybrid copper halides, *Nano Lett.*, 2022, **22**, 846–852.

21 F. Ge, B. H. Li, P. X. Cheng, G. Li, Z. F. Ren, J. L. Xu and X. H. Bu, Chiral hybrid copper(I) halides for high efficiency second harmonic generation with a broadband transparency window, *Angew. Chem., Int. Ed.*, 2022, **61**, e202115024.

22 J. J. Wu, Y. Guo, J. L. Qi, W. D. Yao, S. X. Yu, W. L. Liu and S. P. Guo, Multi-Stimuli Responsive Luminescence and Domino Phase Transition of Hybrid Copper Halides with Nonlinear Optical Switching Behavior, *Angew. Chem., Int. Ed.*, 2023, **62**, e202301937.

23 T. Liu, J. Qin, G. Zhang, T. Zhu, F. Niu, Y. Wu and C. Chen, Mercury bromide ($HgBr_2$): a promising nonlinear optical material in IR region with a high laser damage threshold, *Appl. Phys. Lett.*, 2008, **93**, 091102.

24 Y. Dang, X. Meng, K. Jiang, C. Zhong, X. Chen and J. G. Qin, A promising nonlinear optical material in the Mid-IR region: new results on synthesis, crystal structure and properties of noncentrosymmetric β-HgBrCl, *Dalton Trans.*, 2013, **42**, 9893–9897.

25 Q. Wu, X. Liu, Y. S. Du, C. L. Teng and F. Liang, Nonlinear organic–inorganic halide hybrids containing unprecedented linear $[MIX_2]^-$ coordination units and quasi-two-dimensional lone pairs, *Chem. Commun.*, 2020, **56**, 4894–4897.

26 T. T. Xu, Y. Y. Li, M. Nikl, R. Kucerkova, Z. Y. Zhou, J. Chen, Y. Y. Sun, G. D. Niu, J. Tang, Q. Wang, G. H. Ren and Y. T. Wu, Lead-free zero-dimensional organic-copper(I) halides as stable and sensitive X-ray scintillators, *ACS Appl. Mater. Interfaces*, 2022, **14**, 14157–14164.

27 L. Y. Lian, X. Wang, P. Zhang, J. S. Zhu, X. W. Zhang, J. B. Gao, S. Wang, G. J. Liang, D. L. Zhang, L. Gao, H. S. Song, R. Chen, X. Z. Lan, W. X. Liang, G. D. Niu, J. Tang and J. B. Zhang, Highly luminescent zero-dimensional organic copper halides for X-ray scintillation, *J. Phys. Chem. Lett.*, 2021, **12**, 6919–6926.

28 H. Peng, Y. Tian, X. X. Wang, T. T. Dong, Z. M. Yu, Y. Xiao, Z. H. Zhang, J. P. Wang and B. S. Zou, Highly efficient broadband green emission of $(TPA)CuCl_2$ single crystals: understandingthe formation of self-trapped states, *J. Phys. Chem. C*, 2022, **126**, 8545–8552.

29 S. Q. Chen, J. M. Gao, J. Y. Chang, Y. Q. Li, C. X. Huangfu, H. Meng, Y. Wang, G. J. Xia and L. Feng, Family of highly luminescent pure ionic copper(I) bromide based hybrid materials, *ACS Appl. Mater. Interfaces*, 2019, **11**, 17513–17520.

30 H. Peng, X. Wang, Y. Tian, T. Dong, Y. Xiao, T. Huang, Y. Guo, J. Wang and B. Zou, Water-Stable Zero-Dimensional $(C_4H_9)_4NCuCl_2$ single crystal with highly efficient broadband green emission, *J. Phys. Chem. Lett.*, 2021, **12**, 6639–6647.

31 H. Peng, Y. Tian, Z. Zhang, X. Wang, T. Huang, T. Dong, Y. Xiao, J. Wang and B. Zou, Bulk assembly of zero-dimensional organic copper bromide hybrid with bright self-trapped exciton emission and high antiwater stability, *J. Phys. Chem. C*, 2021, **125**, 20014–20021.

32 S. Andersson and S. Jagner, Crystal structure of ethyltriphenylphosphonium dibromocuprate (I), $[P(C_2H_5)(C_6H_5)_3][CuBr_2]$, *Acta Chem. Scand.*, 1985, **39**, 515–521.

33 D. A. Popy, T. D. Creason, Z. Zhang, D. J. Singh and B. Saparov, Electronic structures and optical properties of $(Ph_4P)MX_2$ (M = Cu, Ag; X = Cl, Br), *J. Solid State Chem.*, 2022, **316**, 123626.

34 G. V. Noshchenko, N. F. Salivon, B. Zarychta and V. V. Olijnyk, Crystal structures of allyltriphenyl-phosphonium halogenocuprates(I), *J. Struct. Chem.*, 2013, **54**, 129–133.

35 O. V. Dolomanov, L. J. Bourhis, R. J. Gildea, J. A. K. Howard and H. Puschmann, OLEX2: a complete structure solution, refinement and analysis program, *J. Appl. Crystallogr.*, 2009, **42**, 339–341.

36 S. K. Kurtz and T. T. Perry, A powder technique for the evaluation of nonlinear optical materials, *J. Appl. Phys.*, 1968, **39**, 3798–3813.

37 M. D. Segall, P. J. D. Lindan, M. J. Probert, C. J. Pickard, P. J. Hasnip, S. J. Clark and M. C. Payne, First-principles simulation: ideas, illustrations and the CASTEP code, *J. Phys.: Condens. Matter*, 2002, **14**, 2717–2744.

38 J. P. Perdew, K. Burke and M. Ernzerhof, Generalized gradient approximation made simple, *Phys. Rev. Lett.*, 1996, **77**, 3865–3868.

39 S. F. Li, X. M. Jiang, B. W. Liu, D. Yan, C. S. Lin, H. Y. Zeng and G. C. Guo, Superpolyhedron-built second harmonic generation materials exhibit large mid-infrared conversion efficiencies and high laser-induced damage thresholds, *Chem. Mater.*, 2017, **29**, 1796–1804.

40 X. M. Jiang, G. E. Wang, Z. F. Liu, M. J. Zhang and G. C. Guo, Large Mid-IR second-order nonlinear-optical effects designed by the supramolecular assembly of different bond types without IR absorption, *Inorg. Chem.*, 2013, **52**, 8865–8871.

41 H. Chan, Y. Chen, M. Dai, C.-N. Lü, H.-F. Wang, Z.-G. Ren, Z.-J. Huang, C.-Y. Ni and J.-P. Lang, Multi-dimensional iodocuprates of 4-cyanopyridinium and N,N′-dialkyl-4,4′-bipyridinium: syntheses, structures and dielectric properties, *CrystEngComm*, 2012, **14**, 466–473.

42 Y. Chen, Z.-O. Wang, Z.-G. Ren, H.-X. Li, D.-X. Li, D. Liu, Y. Zhang and J.-P. Lang, Solvothermal stepwise formation of cu/i/s-based semiconductors from a three-dimensional net to one-dimensional chains, *Cryst. Growth Des.*, 2009, **9**, 4963–4968.

43 X. Liu, W. L. Xu, S. R. Xu, X. Yu, Y. Q. Deng, X. H. Wu, F. Liang and Q. Wu, A series of organic–inorganic hybrid compounds $[(C_2H_5)_4N]InCl_{4-x}Br_x$ (x = 0, 2, 4): synthesis, crystal structure, and nonlinear optical properties, *Inorg. Chem.*, 2020, **59**, 5721–5727.

44 Y. Guo, J. J. Wu, W. L. Liu and S. P. Guo, Organic cation modulation triggered second harmonic response in manganese halides with bright fluorescence, *Inorg. Chem.*, 2022, **61**, 11514–11518.

45 X. Liu, C. M. Ji, Z. Y. Wu, L. N. Li, S. G. Han, Y. Y. Wang, Z. H. Sun and J. H. Luo, $[C_5H_{12}N]SnCl_3$: A tin halide organic–inorganic hybrid as an above-room-temperature solid-state nonlinear optical switch, *Chem. – Eur. J.*, 2019, **25**, 2610–2615.

46 L. L. Chu, T. Zhang, Y. F. Gao, W. Y. Zhang, P. P. Shi, Q. Ye and D. W. Fu, Fluorine substitution in ethylamine triggers second harmonic generation in noncentrosymmetric crystalline $[NH_3CH_2CH_2F]_3BiCl_6$, *Chem. Mater.*, 2020, **32**, 6968–6974.

47 Z. Y. Wu, X. T. Liu, C. M. Ji, L. N. Li, S. S. Wang, Z. H. Sun, W. C. Zhang, Y. Peng and J. H. Luo, Above-room-temperature switching of quadratic nonlinear optical properties in a Bi–halide organic–inorganic hybrid, *J. Mater. Chem. C*, 2018, **6**, 9532–9536.

48 Z. Ma, J. Hu, R. Sa, Q. Li, Y. Zhang and K. Wu, Screening novel candidates for mid-IR nonlinear optical materials from I3–V–VI4 compounds, *J. Mater. Chem. C*, 2017, **5**, 1963–1972.

49 Q. R. Shui, H. X. Tang, R. B. Fu, Y. B. Fang, Z. J. Ma and X. T. Wu, $Cs_3Pb_2(CH_3COO)_2X_5$ (X=I, Br): halides with strong second-harmonic generation response induced by acetate groups, *Angew. Chem., Int. Ed.*, 2021, **60**, 2116–2119.

50 J. J. Wu, Y. Guo, W. D. Yao, W. L. Liu and S. P. Guo, Symmetry breaking of $A_3M_2X_9$-type perovskite derivatives induced by polar quaternary ammonium cations: achieving efficient nonlinear optical properties, *Dalton Trans.*, 2022, **51**, 4878–4883.

51 C. Zhou, H. Lin, H. Shi, Y. Tian, C. Pak, M. Shatruk, Y. Zhou, P. Djurovich, M.-H. Du and B. Ma, A zero-dimensional organic seesaw-shaped tin bromide with highly efficient strongly stokes-shifted deep-red emission, *Angew. Chem., Int. Ed.*, 2018, **57**, 1021–1024.

52 F. F. Wu, Q. Y. Wei, X. Q. Li, Y. Liu, W. Q. Huang, Q. Chen, B. X. Li, J. H. Luo and X. T. Liu, Cooperative enhancement of second harmonic generation in an organic–inorganic hybrid antimony halide, *Cryst. Growth Des.*, 2022, **22**, 3875–3881.